Guiding of vortices under competing isotropic and anisotropic pinning conditions: Theory and experiment

Oleksiy K. Soroka,[1,*] Valerij A. Shklovskij,[2] and Michael Huth[1]
[1]*Johann Wolfgang Goethe-Universität, Physikalisches Institut, Max-von-Laue-Str. 1, D-60438 Frankfurt am Main, Germany*
[2]*Institute for Theoretical Physics, National Science Center Kharkov Institute of Physics and Technology, 61108 Kharkov, Ukraine and Kharkov National University, Physics Department, 61077 Kharkov, Ukraine*
(Received 12 May 2006; revised manuscript received 27 April 2007; published 6 July 2007)

The influence of tailored anisotropic pinning sites on the nonlinear resistivity tensor in the mixed state of epitaxial thin films of niobium was studied by electronic transport measurements and accompanying theoretical modeling. The thin films were prepared by physical vapor deposition of niobium onto faceted α-alumina substrates. The resistivity tensor of the films was determined in the limit of small current densities at various temperatures close to the critical temperature and in different magnetic fields. In these experiments, the angle between the current and the facet ridges of the substrates was set at five fixed angles between 0° and 90°. Perfect guiding of the vortices along the facet ridges was observed over a wide parameter range. The measured resistivities were in good quantitative agreement with the predictions of the employed stochastic modeling approach.

DOI: 10.1103/PhysRevB.76.014504 PACS number(s): 74.25.Qt, 74.25.Fy, 72.15.Gd, 74.78.Db

I. INTRODUCTION

The mixed-state resistive properties of type-II superconductors are determined by the dynamics of the flux-line array which again are strongly influenced by the distribution of pinning sites. Thus, by tailoring the pinning in an anisotropic fashion, the vortex dynamics can be controlled to a large degree. As a result, the resistivity tensor can be tuned to exhibit unconventional behavior which, in turn, allows for a thorough test of the predictive qualities of any theoretical modeling of the vortex dynamics in the presence of anisotropic pinning. A well-known manifestation of such a pinning anisotropy is the directed motion of vortices along unidirectional planar pinning defects, the so-called guided vortex motion or guiding. In guided motion, the vortices tend to move along the pinning planes even if the external force acting on them is not aligned parallel to these planes. Another important feature is that the longitudinal and transverse magnetoresistivities depend substantially on the angle α between the current density vector $\vec{J}$ and the direction of the pinning planes.

One of the first experimental observations of guided vortex motion in the flux-flow (FF) regime was made by Niessen and Weijsenfeld in 1969.[1] These experiments were performed on cold-rolled sheets of a Nb-Ta alloy. The data were interpreted within a phenomenological model which ignored nonlinear effects in the resistive response of the samples. Especially following the discovery of the high-temperature superconductors, the interest in the influence of anisotropic pinning on the vortex dynamics was renewed for two reasons. First, in many of the currently known high-temperature superconductors, crystallographic twin formation occurs during crystal growth with twin planes oriented parallel to the *c* axis. It was proven that these twin boundaries give rise to anisotropic pinning.[2,3] Second, the layered structure of the high-temperature superconductors defines a system of parallel *ab* planes which represent a set of unidirectional planar defects. These are the source of the so-called intrinsic pinning.[4] In experiments on twinned $YBa_2Cu_3O_{7-\delta}$ single crystals, more subtle effects than guiding could be observed. For example, the longitudinal magnetoresistivity was shown to have an odd component with regard to magnetic-field reversal.[5,6] In the first analysis of these experiments, a phenomenological model of the anisotropic pinning was employed. In other experiments, Pastoriza *et al.*[7] and Berseth and co-workers[8,9] varied the angle α between current and twin planes continuously using an "orientable-current-source" setup.

With regard to theoretical modeling of the magnetoresistive response of a system of vortices in the presence of anisotropic pinning, several studies were published within the past years. An approach based on a two-dimensional stochastic model for the vortex dynamics was introduced by Mawatari.[10,11] This model is based on the Fokker-Planck equation for the probability density and probability flux density of the single vortex position. This approach takes into account the stochastic properties of thermal fluctuations in vortex position and allows the deduction of the temperature dependence of the magnetoresistive response of the system. This stochastic model was developed further by Shklovskij *et al.* in Refs. 12–17.

Two difficulties arise when performing studies of anisotropic pinning. First, for materials with short coherence length, such as the high-temperature superconductors, pointlike defects tend to be highly pinning active. This gives rise to an isotropic background pinning which can easily mask anisotropy effects. This was shown to occur in epitaxial thin films of $YBa_2Cu_3O_{7-\delta}$ with unidirectional twins.[18] Second, anisotropies in the normal-state resistivity cause current readjustments already in the normal-state which, in turn, result in a changed resistivity tensor.[19] In the present work, both of these difficulties were avoided by employing Nb epitaxial thin films grown onto faceted $\alpha-Al_2O_3(10\bar{1}0)$ substrates. Due to the rather large coherence length in Nb (70–90 nm), pointlike defects are much less pinning active. Furthermore, the normal-state resistivity anisotropy is very small. As will

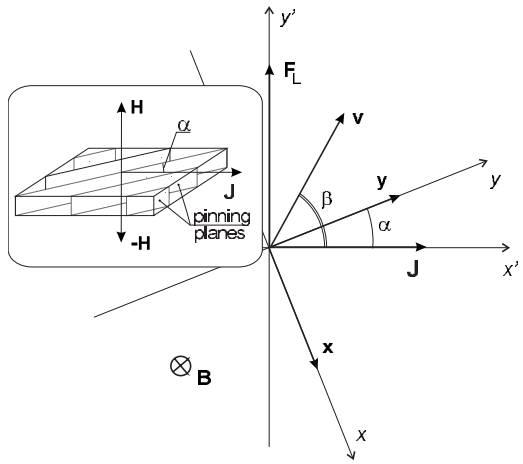

FIG. 1. System of coordinates xy associated with the pinning planes. The anisotropy unit vectors $\hat{x}$ and $\hat{y}$ point perpendicularly and parallel to the pinning planes, respectively. α is the angle between the pinning planes and the dimensionless transport current density vector $\vec{J}$ (see text), β is the angle between the average velocity vector of the vortices $\vec{v}$ and $\vec{J}$ (so-called guiding angle), and $\vec{F}_L$ is the Lorentz force. Inset: Schematic of sample with unidirectional pinning planes in an applied magnetic field $\vec{H}$ giving rise to a macroscopic flux density $\vec{B}$ in the sample.

be shown in the following sections, all effects caused by anisotropic pinning were clearly visible and a quantitative comparison between experiment and theory could be performed.

The organization of the paper is as follows. Section II presents all those theoretical general results in the stochastic model of anisotropic pinning which, for their exposition, do not require a specification of the form of the pinning potential. In Sec. III, details on the sample preparation and the results of the magnetoresistivity measurements are given. The experimental data are analyzed within the theoretical framework in Sec. IV. Section V concludes this paper.

II. THEORETICAL MODEL

A. The Fokker-Planck method in the anisotropic pinning model

We assume that a flat sample with a set of parallel pinning planes is in a magnetic field directed parallel to the pinning planes, as shown in the inset of Fig. 1. A transport current of density $\vec{J}$ flows directed at an angle α to the pinning planes. Longitudinal and transverse resistivities with regard to the current direction are measured for two oppositely directed magnetic fields.

For the theoretical description, the model described in Refs. 10 and 12 is considered here. The Langevin equation for a vortex moving with velocity $\vec{v}$ in the presence of a macroscopic flux density $\vec{B}=\vec{n}B$ ($B=|\vec{B}|$, $\vec{n}=n\hat{z}$, $\hat{z}$ is the unit vector in the z direction, $n=\pm 1$) has the form

$$\eta_0\vec{v} + n\alpha_H[\vec{v}\times\hat{z}] = \vec{F}_L + \vec{F}_p + \vec{F}_{th}. \tag{1}$$

$\vec{F}_L = n\Phi_0\vec{J}\times\hat{z}$ is the Lorentz force per unit length of the vortex and Φ_0 is the magnetic flux quantum. $\vec{F}_p = -\nabla U_p$ is the pinning force with U_p the pinning potential created by the pinning planes. $\vec{F}_{th}$ is the thermal fluctuation force, η_0 is the electronic viscosity, and α_H is the effective Hall coefficient. The fluctuation force $\vec{F}_{th}(t)$ is represented by Gaussian white noise, whose stochastic properties are defined by the relations

$$\langle F_{th,i}(t)\rangle = 0, \quad \langle F_{th,i}(t)F_{th,j}(t')\rangle = 2k_BT\eta_0\delta_{ij}(t-t') \tag{2}$$

at a given temperature T. k_B is the Boltzmann constant. Employing the relations in Eq. (2), Eq. (1) can be reduced to a system of Fokker-Planck equations:

$$\frac{\partial P}{\partial t} = -\nabla\cdot\vec{S}, \tag{3}$$

$$\eta_0\vec{S} + n\alpha_H\vec{S}\times\hat{z} = (\vec{F}_L + \vec{F}_p)P - k_BT\nabla P. \tag{4}$$

Equation (3) reflects continuity of the probability density $P(\vec{r},t)$ associated with finding the vortex at the point $\vec{r}=(x,y)$ at time t. Equation (4) specifies the probability flux density of the vortex $\vec{S}(\vec{r},t)\equiv P(\vec{r},t)\vec{v}(\vec{r},t)$. The definition of the mean vortex velocity is as follows:

$$\langle\vec{v}\rangle = \frac{\int\int \vec{S}d^2r}{\int\int Pd^2r}. \tag{5}$$

Since the anisotropic pinning potential is assumed to depend only on the x coordinate and is furthermore assumed to be periodic [$U_p \equiv U_p(x) = U_p(x+a)$, where a is the period], the pinning force is always directed along the anisotropy axis $\hat{x}$ so that it has no component along the $\hat{y}$ axis ($F_{py} = -dU_p/dy = 0$). This then implies that P and $\vec{S}$ are only functions of x and Eq. (4) in the stationary case for the functions $P=P(x)$ and $\vec{S}=[S_x(x),S_y(x)]$ reduces to the following equations:

$$\eta_0 S_x + n\alpha_H S_y = \left(F_{Lx} - \frac{dU_p}{dx}\right)P - k_BT\frac{dP}{dx}, \tag{6}$$

$$-n\alpha_H S_x + \eta_0 S_y = F_{Ly}P. \tag{7}$$

Eliminating S_y from Eqs. (6) and (7) and omitting terms of the order $\mathcal{O}(\alpha_H^2)$, one obtains

$$k_BT\frac{dP}{dx} + \left(-F_a + \frac{dU_p}{dx}\right)P = -\eta_0 S_x, \tag{8}$$

setting $F_a \equiv F_{Lx} - n\epsilon F_{Ly}$ with the dimensionless Hall coefficient $\epsilon \equiv \alpha_H/\eta_0$ for which it is assumed $\epsilon \ll 1$. From the mathematical point of view, Eq. (8) is the Fokker-Planck equation of the one-dimensional vortex dynamics.[20,21] Thus, the problem of two-dimensional vortex motion reduces to a one-dimensional problem in which a combination of the x and y components of the Lorentz force enters as the external force,

$$F_a = n\Phi_0(J_y + n\epsilon J_x) = n\Phi_0(\cos\alpha + n\epsilon \sin\alpha)J. \quad (9)$$

In the stationary case, continuity [cf. Eq. (3)] demands that $dS_x/dx=0$, and thus S_x is independent of x. By direct integration, the solution of Eq. (8) for periodic boundary conditions $P(0)=P(a)$ and a pinning potential of the general form is

$$P(x) = \frac{\eta_0 S_x}{k_B T}\frac{f(a)f(x)}{f(a)-f(0)}\int_x^{x+a}\frac{d\xi}{f(\xi)}, \quad (10)$$

with $f(x)=\exp[[F_a x - U_p(x)]/k_B T]$. Hence, one obtains an expression for the x component of the vortex mean velocity by employing Eq. (5),

$$\langle v_x\rangle = \frac{F_a \nu_a(F_a)}{\eta_0}, \quad (11)$$

with

$$\frac{1}{\nu_a(F_a)} \equiv \frac{F_a}{k_B T a[1-\exp(-F_a a/k_B T)]}\int_0^a dx\int_0^a dx' \times\exp\left(-\frac{F_a x}{k_B T}\right) \times\exp\left[\frac{U_p(x+x')-U_p(x')}{k_B T}\right]. \quad (12)$$

The dimensionless function $\nu_a(F_a)$ in the limit $F_a\to 0$ coincides with the analogous quantity introduced in Ref. 10. It has the physical meaning of the probability of the vortex, being located on a pinning plane, to overcome the potential barrier, the characteristic value of which is denoted as U_0. This can be seen by considering the limiting cases of high ($k_B T \gg U_0$) and low ($k_B T \ll U_0$) temperatures. In the case of high temperatures, $\nu_a \approx 1$ and Eq. (11) corresponds to the FF regime. In this case, the influence of pinning can be neglected. In the case of low temperatures, ν_a is a function of the current. For strong currents, the potential barrier disappears, leading to $\nu_a \approx 1$, and again, the FF regime is realized. For small currents, ν_a takes on the form $\nu_a \sim \exp(-U_0/k_B T)$, which corresponds to the regime of thermally activated flux flow (TAFF).[4] The transition from the TAFF regime to the FF regime is associated with a lowering of the potential barrier with increase of the current.

B. Probability function and the average pinning force

The physical meaning of the ν_a function is the probability of the vortex to jump over a pinning barrier. There exists another physical interpretation and it is shown below that the ν_a function has a close relationship to the average pinning force acting on the vortex.

Neglecting the Hall effect, one can average Eq. (1) as follows:

$$\eta_0\langle\vec{v}\rangle = \langle\vec{F}_L\rangle + \langle\vec{F}_p\rangle. \quad (13)$$

Because the pinning potential U is a function of the x coordinate only, the same holds true for the pinning force $\vec{F}_p = \vec{F}_p(x)$, and thus

$$\eta_0\langle v_x\rangle = F_{Lx} + \langle F_p\rangle,$$

$$\eta_0\langle v_y\rangle = F_{Ly}. \quad (14)$$

On the other hand, again for $\epsilon=0$,

$$\eta_0\langle v_x\rangle = F_{Lx}\nu_a(F_{Lx}),$$

$$\eta_0\langle v_y\rangle = F_{Ly}. \quad (15)$$

The first equation follows directly from Eq. (11) and the second equation is obtained by integration of Eq. (7) taking into account the definition of the average velocity, Eq. (5). Comparing now Eqs. (14) and (15), it is evident that the average pinning force acting on the vortex is connected to the ν_a function in an easy way,

$$\langle F_p\rangle = -F_{Lx}(1-\nu_a). \quad (16)$$

The ν_a function is a probability function so it always fulfills the condition $0\leqslant\nu_a\leqslant 1$. There are two limiting cases for this function. The condition $\nu_a=1$ corresponds to the case when the probability of the vortex to jump across the pinning barrier is equal to 1 and the pinning barriers do not affect the vortex motion any more. Accordingly, the average pinning force is equal to zero, as is evident from Eq. (16). For $\nu_a=0$, the probability for the vortex to jump across the pinning barrier is zero. The average pinning force acting on the vortex is maximal and equal to $-F_{Lx}$ according to Eq. (16).

The dependence of the guiding angle β on the ν_a function is also evident from Eq. (15). The magnitude of this angle can be deduced from the ratio v_x/v_y. It is easy to see that the velocity component v_x increases in conjunction with ν_a, and thus the guiding angle increases, too. If $\nu_a=0$, guiding is always perfect and the vortices move along the pinning planes.

C. The nonlinear conductivity and resistivity tensors

The electric field induced by a moving vortex system is

$$\vec{E} = \vec{B}\times\langle\vec{v}\rangle = nB(-\langle v_y\rangle\hat{x} + \langle v_x\rangle\hat{y}), \quad (17)$$

which we write in components,

$$E_x = -nB\langle v_y\rangle,$$

$$E_y = nB\langle v_x\rangle. \quad (18)$$

Using Eqs. (5) and (7), in conjunction with Eq. (17), we obtain the following simple linear relation between the electric-field components E_x and E_y and the transport current density J_x:

$$E_x + n\epsilon E_y = \rho_f J_x, \quad (19)$$

with the average resistivity $\rho_f \equiv \Phi_0 B/\eta_0$ in the FF regime. From Eqs. (11), (18), and (19) now follows the current-voltage characteristics in the xy coordinate system,

$$e_x = j_x - \epsilon\nu_a(f)f, \quad (20)$$

$$e_y = n\nu_a(f)f, \tag{21}$$

in which the dimensionless components of the electric field are measured in units of $E_0=BU_0/(a\eta_0)$ and the current in units of $J_0=U_0/(\Phi_0 a)$. We furthermore have $f=F_a a/U_0 = nj_y+\epsilon j_x$ according to Eq. (9). Neglecting terms of the order $\mathcal{O}(\epsilon^2)$, we read off the resistivity tensor $\hat{\rho}(\vec{j})$ whose components are measured in units of ρ_f,

$$\hat{\rho} = \begin{pmatrix} \rho_{xx} & \rho_{xy} \\ \rho_{yx} & \rho_{yy} \end{pmatrix} = \begin{pmatrix} 1 & -n\epsilon\nu_a \\ n\epsilon\nu_a & \nu_a \end{pmatrix}, \tag{22}$$

in which all but the ρ_{xx} component depend on the electric current. The conductivity tensor $\hat{\sigma}$, which is the inverse tensor to $\hat{\rho}$, has the form

$$\hat{\sigma} = \begin{pmatrix} \sigma_{xx} & \sigma_{xy} \\ \sigma_{yx} & \sigma_{yy} \end{pmatrix} = \begin{pmatrix} 1 & n\epsilon \\ -n\epsilon & 1/\nu_a(f) \end{pmatrix} \tag{23}$$

and is measured in units of $1/\rho_f$. Again, we neglected terms of the order $\mathcal{O}(\epsilon^2)$.

For the following discussion, it is convenient to introduce the L and T geometries in which $\vec{j}\parallel\hat{x}$ and $\vec{j}\perp\hat{x}$, respectively. If one neglects the Hall terms in Eq. (22) (i.e., $\epsilon\to 0$), then in the L geometry, vortex motion takes place along the pinning planes, and in the T geometry, transverse to the pinning planes. In the L geometry, the critical current is equal to zero since the FF regime is realized for guided vortex motion along the pinning planes.[42] In the T geometry, a pronounced nonlinear regime is realized for $k_BT \ll U_0$.

The experimentally measured quantities are referenced with regard to the coordinate system associated with the current (see Fig. 1). The longitudinal and transverse components of the electric field relative to the direction of the current, $e_\parallel$ and $e_\perp$, respectively, are related in a simple way to e_x and e_y:

$$e_\parallel = e_x \sin\alpha + e_y \cos\alpha, \tag{24}$$

$$e_\perp = -e_x \cos\alpha + e_y \sin\alpha. \tag{25}$$

The field $e_\parallel(j,\alpha)$ as a function of j for α=const is monotonically increasing and reduces to $e_\parallel=e_x(j)$ for $\alpha=\pi/2$ (the L geometry) and to $e_\parallel=e_y(j)$ for $\alpha=0$ (the T geometry). The field $e_\perp(j,\alpha)$ as a function of j for α=const exhibits a pronounced nonlinearity and has an extremum associated with the guiding effect.

D. Influence of additional pointlike pinning on the guided vortex motion

Up to now, only anisotropic pinning produced by the parallel pinning planes was taken into account. The absence of isotropic pinning leads to the absence of a critical current for all current directions with respect to the pinning planes, except for $\alpha=0$. To remedy this obvious discrepancy with regard to the experimental observations, an isotropic pinning caused by uncorrelated pointlike defects must also be considered. In this chapter, a short summary of an extension of the described theoretical model on anisotropic pinning is given.

In the presence of uncorrelated pointlike defects, each vortex moving with velocity $\vec{v}$ is subject to an isotropic pinning force $\vec{F}_p^i$ which can be formulated as

$$\vec{F}_p^i = -\eta_i(v)\vec{v}, \tag{26}$$

with $\eta_i(v)$ being a velocity-dependent viscosity and $v=|\vec{v}|$.[22] The Langevin equation for vortex motion [Eq. (1)] must be modified in this case as follows:

$$\eta_0\vec{v} + n\alpha_H[\vec{v}\times\hat{z}] = \vec{F}_L + \vec{F}_p^a + \vec{F}_p^i + \vec{F}_{th}. \tag{27}$$

With Eq. (26), this reduces to

$$\eta\vec{v} + n\alpha_H[\vec{v}\times\hat{z}] = \vec{F}_L + \vec{F}_p^a + \vec{F}_{th}, \tag{28}$$

with $\eta=\eta(v)\equiv\eta_0+\eta_i(v)$. It was shown in Ref. 23 that using the results from the previous section, the solution of Eq. (28) can be written in the form

$$\eta_0\langle\vec{v}\rangle = \nu_i(F_I)\vec{F}_I, \tag{29}$$

in which the vector $\vec{F}_I$ has the following components:

$$F_{Ix} = F_a\nu_a(F_a),$$

$$F_{Iy} = F_{Ly} + n\tilde{\epsilon}F_a\nu_a(F_a). \tag{30}$$

Here, F_a is given as $F_a\equiv F_{Lx}-n\tilde{\epsilon}F_{Ly}$ and $F_I=\sqrt{F_{Ix}^2+F_{Iy}^2}$. We furthermore introduced $\tilde{\epsilon}\equiv\epsilon\nu_i(F_i)$ and $F_i\equiv F_I(\epsilon=0)$ assuming again $\epsilon\ll 1$. All the subsequent results are given in this limit. The functions $\nu_i=\eta_0/\eta(v)$ and ν_a have the physical meaning of the probability to overcome the isotropic and anisotropic pinning barriers, respectively. Both ν_i and ν_a can be calculated using a simple triangle model potential as described earlier[12] with different potential depths U_0, periods a, and characteristic widths b for isotropic and anisotropic pinnings, respectively.

Analogous to the previous section, the even and odd components of the longitudinal and transverse magnetoresistivities, measured in units of ρ_f and defined by the relations $\rho^\pm=[\rho(n)\pm\rho(-n)]/2$, were calculated in Refs. 23 and 24. We present these in a compact and convenient form as follows:

$$\rho_\parallel^+ = \nu_i(F_i)\cdot\rho_{\parallel a}^+, \quad \rho_\perp^+ = \nu_i(F_i)\cdot\rho_{\perp a}^+, \tag{31}$$

and

$$\rho_\parallel^- = \nu_i^-\rho_{\parallel a}^+ + \nu_i^2(F_i)\cdot\rho_{\parallel a}^-,$$

$$\rho_\perp^- = \nu_i^2(F_i)\cdot\rho_{\perp a}^- - \frac{1}{2}\rho_f\nu_i^-(1-\nu_a)\sin 2\alpha. \tag{32}$$

Here, ν_i^- and ν_a^- are the odd components of the probability functions $\nu_i(F_I)$ and $\nu_a(F_a)$, respectively. Furthermore, we note $\nu_i^-=\nu_i^-[F_I(n)]$ and $F_I(n)=[F_{Ly}^2+F_{Lx}^2\nu_a^2(F_a) + 2n\epsilon\nu_i(F_i)F_{Lx}F_{Ly}\nu_a(1-\nu_a)]^{1/2}$.

According to this result, what is the influence of isotropic pinning on the guiding effect? The guiding angle β is given by $\cot\beta=-\rho_\perp^+/\rho_\parallel^+$, as is shown in Ref. 12. From Eq. (31), we readily see that

$$\cot\beta = -\frac{\rho_{\perp}^{+}}{\rho_{\parallel}^{+}} = -\frac{\rho_{\perp a}^{+}}{\rho_{\parallel a}^{-}}. \tag{33}$$

From this, we conclude that the guiding angle β is not influenced by the isotropic disorder. Isotropic pinning therefore influences only the magnitude of the vortex velocity but not its direction.[24]

III. EXPERIMENT

For the experimental realization of the anisotropic pinning scenario discussed so far, two aspects have to be considered. First, in order to obtain a most clear expression of the effects of anisotropic pinning, the isotropic pinning contribution must not dominate the vortex dynamics. This means that it must be possible to prepare the samples with sufficient structural and chemical purity. Second, it must be secured that the influence of current guiding effects due to the anisotropic resistance, as, e.g., shown to exist in numerical simulations of driven vortex systems,[19] can be neglected in comparison with the vortex guiding effects.

We chose epitaxial Nb thin films grown on the faceted surface of $(10\bar{1}0)$-cut (m-plane) α-Al_2O_3 in our experiments. For the refractory $3d$ metals Mo, Nb, and Ta, a complete three-dimensional epitaxial relationship for the growth on low-index surfaces of α-Al_2O_3 is established.[25] Thin films can be grown with excellent structural quality. Since Nb has a body-centered-cubic structure, its normal-state conductivity is isotropic. Finally, the $3d$ refractory metals coherently overgrow the faceted m-plane surface of α-Al_2O_3,[26] which implies that grain-boundary scattering effects in the Nb films for current flow perpendicular to the facet ridges is not an issue. Consequently, we considered our experimental approach to be a valid testing ground for vortex guiding effects.

A. Sample preparation

It is known that the surfaces of metals, semiconductors, and ceramics can exhibit a faceted hill-and-valley structure.[27–30] This can result from external perturbations, such as chemical adsorption on the previously flat surface or as the result of the surface being thermodynamically unstable. The first explanation for the driving force of this process was given by Herring.[31] According to his reasoning, all surfaces other than those found on the equilibrium crystal shape will decompose into a hill-and-valley structure in order to reduce the overall surface free energy. A detailed recent account of this phenomenon can be found in Ref. 32.

$(10\bar{1}0)$-cut (m-plane) α-Al_2O_3, as employed here, develops a semiperiodic faceted surface when annealed at high temperatures in air.[33] It is known that this surface forms an excellent template for the growth of epitaxial Nb, Mo, and Fe layers.[26,34–36] Roughly speaking, the large surface energy of the $(10\bar{1}0)$ surface drives a hill-and-valley structure formation consisting of the $(10\bar{1}1)$ and $(10\bar{1}\bar{2})$ planes.[37,38] In fact, the $(10\bar{1}\bar{2})$ plane is an approximant to the true, slightly curved surface, as was observed in cross-section transmission electron microscopy studies.[26] The faceted substrate surface is schematically shown in the inset of Fig. 2. The $(10\bar{1}1)$ and $(10\bar{1}\bar{2})$ surfaces form the angles of 17.6° and 32.4° with the $(10\bar{1}0)$ plane of α-Al_2O_3, respectively.[26] In previous work, it was shown that the facets exhibit an average periodicity of 400 nm with aspect ratios (height-to-period length) of about 1:8.[34] The Nb films grown on these substrates to a thickness of 25 nm using molecular beam epitaxy techniques replicate the faceted substrate surface, as shown in Fig. 2. The facet ridges act as effective pinning planes. For details concerning the growth, we refer to Refs. 34 and 39.

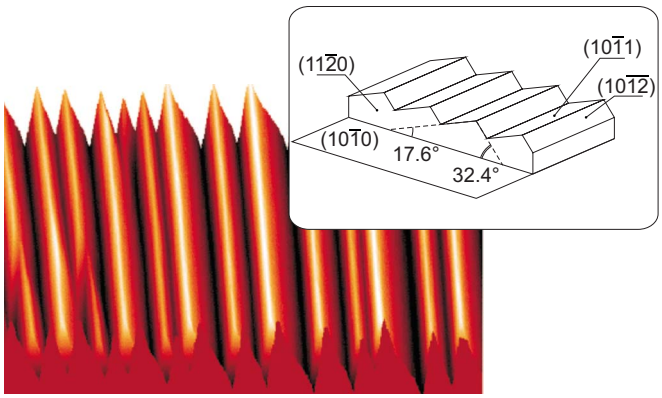

FIG. 2. (Color online) STM image of Nb film deposited on the faceted α-Al_2O_3 substrate surface. Data were taken at 1.0 V bias with a current of 1 nA. Scan ranges are 500 nm (lateral) and 50 nm (height). Inset: Faceted surface of the $(10\bar{1}0)$-Al_2O_3 substrate.

For all resistivity measurements, the standard four-probe technique was used. Well defined geometries are required for measurements of the longitudinal and transverse magnetoresistivities of the samples. For this purpose, the Nb films were patterned, after deposition and structural characterization, by means of contact photolithography with subsequent ion-beam etching. The thus obtained structure consisted of five microbridges oriented at different angles α, as shown in the inset of Fig. 3. The microbridges had a width of 25 μm and a length of 510 μm. This structure allowed us to measure the longitudinal and transverse voltages for different transport current directions with respect to the facet ridges at the angles α=0°, 30°, 45°, 60°, and 90° on the same thin-film sample. The patterned samples were wire bonded and mounted on the sample holder of a ^{4}He cryostat with a superconducting solenoid. All the magnetoresistivity measurements were performed in external magnetic fields $+\vec{H}$ and $-\vec{H}$ directed perpendicular to the averaged film surface, and the even and odd magnetoresistivity components were calculated according to the following simple relation:

$$\rho^{\pm} = [\rho(+\vec{H}) \pm \rho(-\vec{H})]/2. \tag{34}$$

B. Magnetoresistivity measurements

The measurements presented below were performed on one Nb thin-film sample. Selected measurements were repeated on a second sample of equal thickness and structural quality to confirm the reproducibility of the results. A trans-

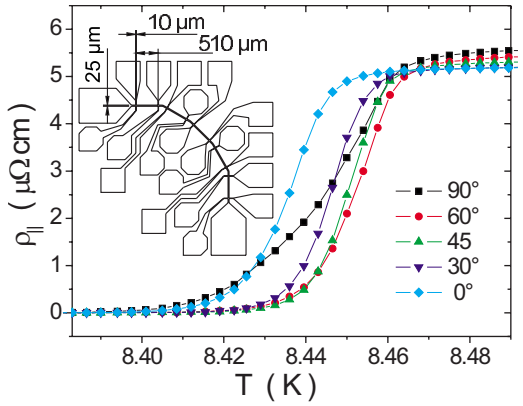

FIG. 3. (Color online) Superconductive transition in zero magnetic field for the different transport current orientations with respect to the facet ridges, as indicated. Inset: Hall structure as used for the magnetoresistivity measurements. The structure allows to send a transport current at the angles of 0°, 30°, 45°, 60°, and 90° with respect to a predefined direction.

port current density of 8 kA/cm^2 was chosen for all measurements.

The superconductive transition for the different current orientations is shown in Fig. 3. The critical temperature in zero magnetic field is T_c=8.46 K with a transition width of about 0.04 K. Due to the faceted film surface, different normal-state resistances for the microbridges oriented at different angles to the facets are expected. The same holds true for the calculated resistivities which were obtained by assuming microbridge dimensions of 510 μm (length) and 25 μm (width) irrespective of their orientation with regard to the facet ridges. For α=0°, the transport current flows parallel to the facet ridges, so the effective width of the bridge is about 10% larger as compared to a bridge patterned on a flat film. For α=90° orientation, the current flows perpendicular to the facets, so the effective length of the bridge is about 10% larger in this case. From this follows that the normal-state resistivity should be larger by about 20% for α=90° as compared to the resistivity for α=90°. This agrees qualitatively with the experimental data shown in Fig. 3. Quantitatively, the measured difference amounts to 7%. The explanation for this is that any given facet ridge does not extend through the whole microbridge as it was assumed in the simple estimate above. Instead, there exist defects in the facet structure where the convex and concave facet ridges gradually change place.[34] In these regions, the substrate surface is flatter which will tend to reduce the apparent resistivity differences.

The temperature dependence of the even component of the longitudinal resistivity $\rho_{\parallel}^{+}$ in a magnetic field of $\mu_0 H$ =15 mT is shown in Fig. 4. The curves show very good systematic behavior. The dependence of the normal-state resistivity on the angle α can be stated with the following relations which can be derived within the described theoretical model in the FF regime at the border to the normal state:

$$\rho_{\parallel N}(\alpha) = \rho_N(1 - \Delta \cos 2\alpha), \tag{35}$$

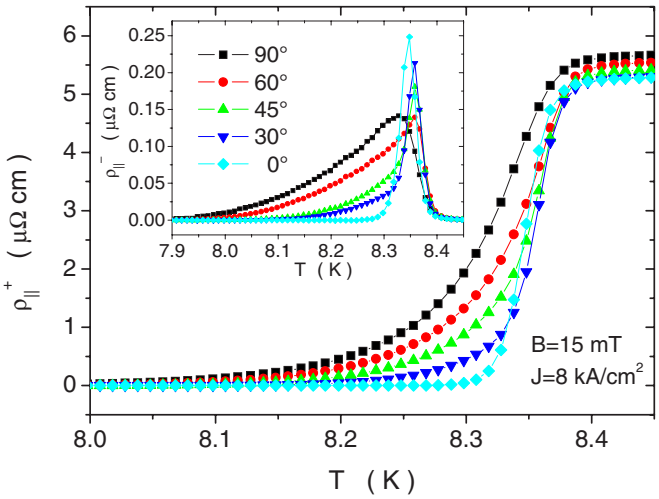

FIG. 4. (Color online) Temperature dependence of the even longitudinal $\rho_{\parallel}^{+}$ and odd longitudinal $\rho_{\parallel}^{-}$ (inset) magnetoresistivity components for the different transport current orientations with respect to the facet ridges, as indicated.

$$\rho_{\perp N}(\alpha) = -\Delta \rho_N \sin 2\alpha, \tag{36}$$

in which $\rho_N \equiv \rho_{\parallel N}(45°)$ is the longitudinal magnetoresistivity in the normal state for the α=45° transport current orientation and $\rho_{\perp N}(45°)$ is the transverse magnetoresistivity for the transport current directed at an angle α=45°. Δ is defined as $\Delta = -\frac{\rho_{\perp N}(45°)}{\rho_{\parallel N}(45°)}$. These two equations reflect the tensorial behavior of the resistivity components. The measured values of the longitudinal resistivities differ from the calculated ones according to Eq. (35) by only about 0.4% for all measured angles except for α=0°, for which this difference is 2.5%. From Figs. 3 and 4, one can see that the normal-state curves almost coincide for α=0° and 30°, which is most likely due to a small angle misalignment of the microbridge structure with regard to the exact direction of the facet ridge lines. From this good agreement between the experimental data and the theoretical prediction, we extract further confidence that a possible influence of spurious current guiding effects can indeed be excluded.

We now turn to those experimental findings which signify the occurrence of guided vortex motion. First, in the inset of Fig. 4, the temperature dependence of the longitudinal odd component $\rho_{\parallel}^{-}$ for the different angles α is shown. The peak magnitude is maximal for α=0°. The same measurements in magnetic fields $\mu_0 H$=3, 7, 30, 60, and 90 mT show that with increasing magnetic field, all peaks become broader and the peaks for α=0°, 30°, and 45° reduce their amplitude. The appearance of this component is a characteristic feature of the guided vortex motion.[12] Second, the dependence of the even transverse magnetoresistivity component $\rho_{\perp}^{+}$ on the temperature, shown in Fig. 5, demonstrates a maximal magnitude for α=45° and almost zero response for α=0° and 90°. The appearance of this component in the superconductive state is again caused by guided vortex motion. The behavior of all these curves does not qualitatively change while changing the magnetic field. It is again possible to describe

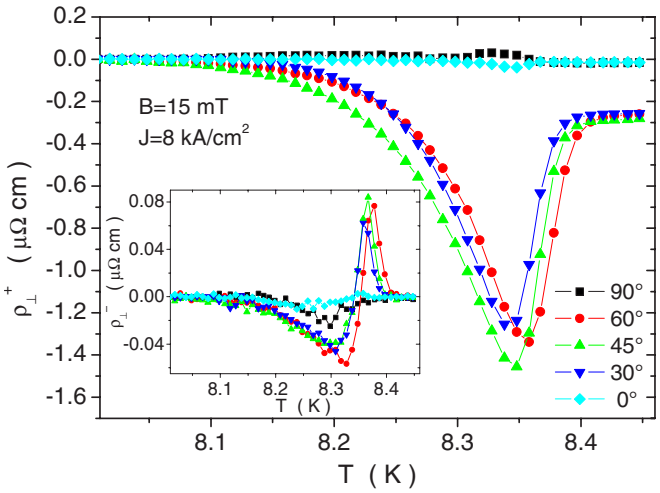

FIG. 5. (Color online) Temperature dependence of the even transverse $\rho_\perp^+$ and odd transverse $\rho_\perp^-$ (inset) magnetoresistivity components for the different transport current orientations with respect to the facet ridges, as indicated.

the anisotropy of this magnetoresistivity in the normal state using relation (36). In particular, according to this relation, the transverse resistivities for the currents oriented at the angles α and $(90°-\alpha)$ must coincide. Indeed, the curves for $\alpha=30°$ and $\alpha=60°$ in Fig. 5 are the same in the normal state ($T>8.4$ K) within the experimental resolution. The measured normal-state resistivities are also in good agreement with the resistivities as calculated using relation (36).

For completeness, we also show the dependence of the odd transverse magnetoresistivity $\rho_\perp^-$ on temperature in the inset of Fig. 5. This quantity shows the so-called anomalous Hall effect: $\rho_\perp^-$ changes its sign from negative to positive with increasing temperature. With increasing magnetic field, the amplitude of the negative peak increases whereas the height of the positive peak decreases. This sign change can be accounted for within our theoretical approach. Nevertheless, it is not possible to associate this feature unequivocally to guiding phenomena since the anomalous Hall effect was also observed in Nb thin films grown on flat surfaces.

We conclude this section by presenting the data in a more intuitive way. In Fig. 6, we show a polar plot of the absolute value of the resistivity as a function of the transport current direction with respect to the facet ridges for the temperature range from 8.01 to 8.40 K. At high temperatures, the data lie on circles. At low temperatures, the vortex motion is affected due to the plane pinning caused by the facet ridges. Accordingly, the form of the curves changes with decreasing temperature and becomes eight shaped with a maximum for the transport current oriented at 90° to the facet ridges. This can be clearly seen in Fig. 6(b). Very similar dependencies were observed by Pastoriza *et al.* in measurements on $YBa_2Cu_3O_{7-\delta}$ single crystals.[7] Since the Lorentz force $\vec{F}_L$ is always oriented perpendicular to the transport current direction and is responsible for the vortex motion, the 90° current orientation corresponds to the vortices moving along the facet ridges, whereas the 0° orientation corresponds to the transverse motion. The observed maximum of the amplitude for the 90° current orientation and the minimum for the 0°

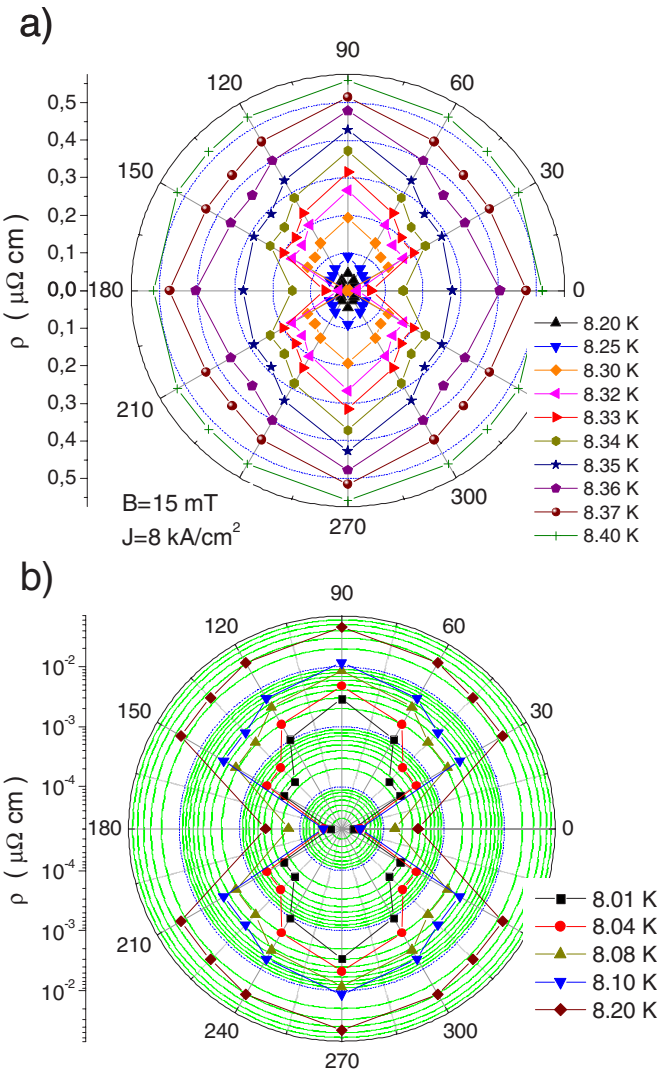

FIG. 6. (Color online) Polar plot of the absolute value of the full resistivity as the transport current is rotated for different temperatures, as indicated.

orientation prove that at low temperatures, the magnetoresistivity is very anisotropic and the vortices prefer to move along the pinning planes (a faster vortex motion corresponds to a larger magnetoresistivity). Such an eight-shaped form of the curves with a maximum for the 90° transport current orientation is a clear signature of a guided vortex motion along the facet ridges.

IV. DISCUSSION OF THE EXPERIMENTAL DATA

A. Guiding in Nb films

We now turn to a more in-depth analysis of the guiding phenomenon in the Nb films. We begin by calculating the guiding angle β from the experimental data employing Eq. (33). The thus determined guiding angle is shown in Fig. 7. Apparently, in the mixed state, the guiding angle β is almost equal to the angle α between the facet ridges and the transport current. This signifies near-perfect guiding in the Nb films. At temperatures near T_c, isotropization of the pinning

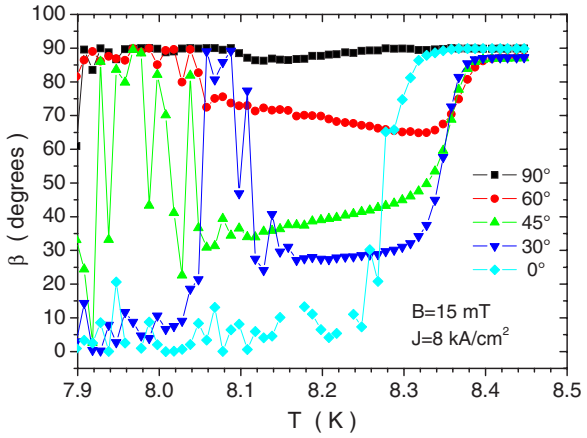

FIG. 7. (Color online) The dependence of the guiding angle β on temperature for different current orientations, as indicated.

is observed. In this region, pinning planes do not affect the vortex motion any more and the vortex velocity tends to be parallel to the Lorentz force, i.e., perpendicular to the transport current direction. Consequently, the guiding angle β becomes equal to 90°.

B. Arrhenius analysis of the even longitudinal resistivity component

In order to quantify the pinning potential that prevents vortex motion across the pinning planes, we performed an Arrhenius analysis. This analysis is applicable if the vortex motion is thermally activated. The resistivity of the sample is then given by Arrhenius' law,

$$\rho = \rho_0 \exp\left(\frac{-U_{\text{eff}}}{k_B T}\right), \tag{37}$$

with ρ_0 a constant and U_{eff} the effective activation energy. The analysis was performed for three different magnetic fields: $\mu_0 H = 7$, 15, and 30 mT. The results appear in

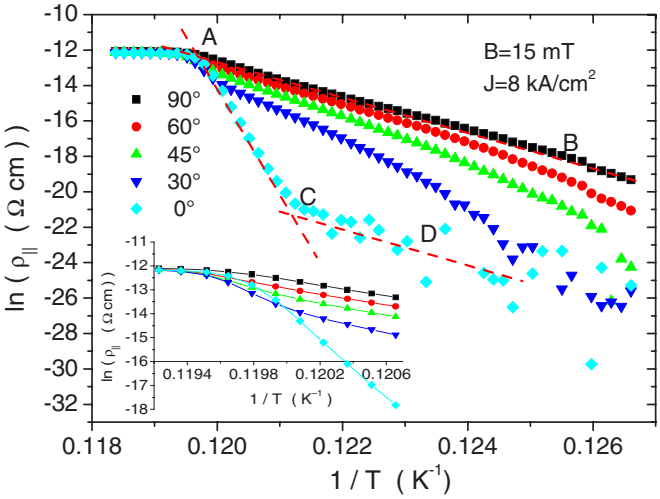

FIG. 9. (Color online) Arrhenius plot of the even longitudinal magnetoresistivity in a magnetic field of $\mu_0 H = 15$ mT for the different transport current orientations with respect to the facet ridges, as indicated. Inset: temperature range of 8.39 K $> T >$ 8.29 K. The dependences for $\alpha = 90°$ and 60° are linear for $1/T > 0.1197$ ($T < 8.36$ K), whereas for $\alpha = 0°$ and 30°, the linear part exists for $1/T > 0.1200$ ($T < 8.33$ K).

Figs. 8–10. The activation energies vs transport current direction, as deduced from the linear parts of Fig. 9 for the field of 15 mT, are compiled in Table I. For comparison, the activation energy for vortex movement across twinning planes in high-temperature superconductors amounts to about 200–3000 K.[40,41]

The Arrhenius representation allows again to exclude any appreciable influence of parasitic current guiding phenomena. From the figures, it is evident that in the superconductive state, the pinning anisotropy plays a much more important role than the anisotropy of the film in the normal state. In fact, the curves practically coincide in the left part of the Arrhenius plots which corresponds to the normal state, whereas in the superconductive state, their behavior is

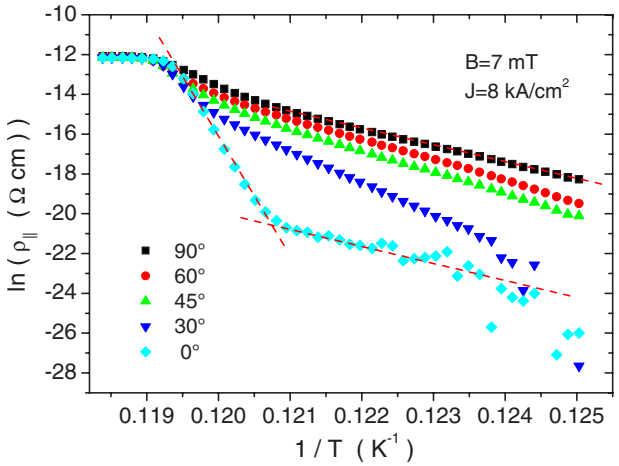

FIG. 8. (Color online) Arrhenius plot of the even longitudinal magnetoresistivity in a magnetic field of $\mu_0 H = 7$ mT for the different transport current orientations with respect to the facet ridges, as indicated.

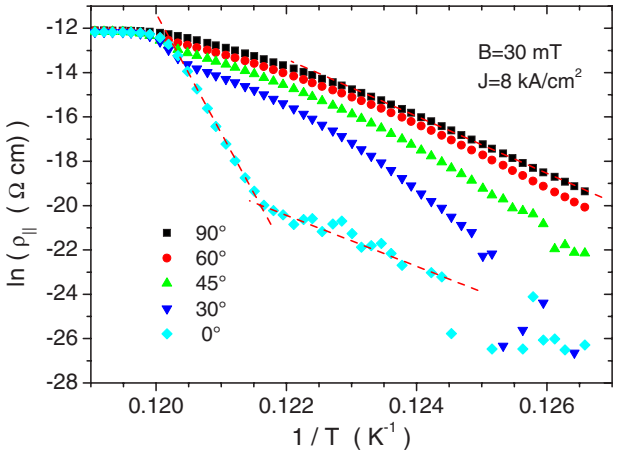

FIG. 10. (Color online) Arrhenius plot of the even longitudinal magnetoresistivity in a magnetic field of $\mu_0 H = 30$ mT for the different transport current orientations with respect to the facet ridges, as indicated.

TABLE I. Activation energies calculated from the linear parts of the Arrhenius plots of the even longitudinal magnetoresistivity in a magnetic field of $\mu_0 H=15$ mT (Fig. 9) for the different transport current orientations with respect to the facet ridges.

Current orientation α (deg)	Activation energy U_{eff} (K)	Temperature range T (K)
90	949	8.08–8.32
60	1032	8.08–8.32
45	1237	8.08–8.32
30	1655	8.12–8.32
0	5599	8.26–8.32

strongly dependent on the transport current orientation with regard to the facet ridges.

We now turn to the more detailed analysis of the Arrhenius representation with regard to our stochastic approach. As described earlier, the even longitudinal magnetoresistivity component is given by the following relation:[43]

$$\rho_{\parallel} = \nu_i \rho_{\parallel a}. \tag{38}$$

Taking the logarithm of this expression, one obtains for $\alpha \neq 90°$ the following:

$$\ln \rho_{\parallel} = \ln \nu_i + \ln(\tan^2 \alpha + \nu_a) + \ln(\rho_f \cos^2 \alpha). \tag{39}$$

The last term in this expression is almost independent of temperature. So, to understand the dependence of $\ln \rho_{\parallel}^{+}$ on temperature, only the temperature dependences of the first two terms in Eq. (39) need to be taken into account.

In the theoretical framework, it can be shown that the probability function ν is proportional to $\exp(-U_0/k_B T)$ in the weak-current limit $Fb \ll U$. F is the external force acting on the vortex. To analyze the behavior of $\ln \rho_{\parallel}$ vs $1/T$, we use the following model function for the representation of ν_i and ν_a:

$$\nu(T,F) = \exp\left(-\frac{\theta U_{\text{eff}}}{k_B T}\right). \tag{40}$$

$\theta = 1 - T/T_c$ is the normalized deviation from the critical temperature. The effective pinning potential is given by $U_{\text{eff}} = U_0 - Fb$ with U_0 as depth of the potential well. In general, both probability functions ν_i and ν_a can be represented by relation (40) with different parameters U_{0i}, U_{0a}, b_i, and b_a and variables F_i and F_a. The subscripts i and a denote the quantities related to isotropic and anisotropic pinnings, respectively.

Let us now consider the curves for the $\alpha=0°$ and $\alpha=90°$ transport current orientations in Arrhenius representation for the magnetic field $\mu_0 H=15$ mT, as shown in Fig. 9. The Arrhenius plot for $\alpha=90°$ can be fitted well by a straight line AB with a slope of 949 K. The curve for $\alpha=0°$ has two linear parts: AC with a slope of 5599 K and CD which is parallel to AB (compare also with Figs. 8 and 10). As can be seen from Eq. (38), the longitudinal resistivity for $\alpha=90°$ is $\rho_{\parallel}(90°)=\rho_f \nu_i$ and

$$\ln \rho_{\parallel}(90°) = \ln \rho_f + \ln \nu_i.$$

Consequently, the slope of the Arrhenius plot is defined only by the probability function ν_i.

On the other hand, for the $\alpha=0°$ transport current orientation from Eq. (39) follows $\ln \rho_{\parallel}(0°) \approx \ln \nu_i + \ln \nu_a$, and thus the slope of the Arrhenius plot is defined by both probability functions, ν_i and ν_a. Since during the lithographic process a small misalignment of the microbridge structures with respect to the facet ridges could not be excluded, the angle α may differ by a small amount $\delta\alpha$ from the nominal value. So, to describe the case $\alpha=0$, one has to use Eq. (39). Let us take a closer look on its second term $\ln(\tan^2 \alpha + \nu_a)$. With decreasing temperature, the probability function $\nu_a \to 0$. So, there exists a temperature region in which even for small α we obtain $\tan^2 \alpha > \nu_a$ for all $\alpha \neq 0$. Because $\tan^2 \alpha$ does not depend on temperature and $\tan^2 \alpha > \nu_a$, one can neglect ν_a in this term when considering the temperature dependence. This means that at low enough temperatures, the temperature dependence of $\ln \rho_{\parallel}$ will be given only by the probability function ν_i,

$$\ln \rho_{\parallel}(0°) \approx \ln \nu_i.$$

This means that the slope of the Arrhenius plot at low enough temperatures will be the same for the $\alpha=0°$ and $\alpha=90°$ orientations if a small deviation of the transport current orientation is present in the measurements. This effect is clearly visible in Figs. 8–10.

We now aim for a complete description of the temperature dependence of the longitudinal resistivity within the stochastic approach. As was shown previously in Refs. 23 and 24, the forces F_a and F_i, which are the arguments of the probability functions ν_a and ν_i, respectively, can be given by the following expressions in the case of a small Hall effect:

$$F_a = F \cos \alpha,$$

$$F_i = F \cos \alpha \sqrt{\tan^2 \alpha + \nu_a^2(T, F_a, \alpha)}. \tag{41}$$

Here $F = F_L \cdot l$ is the Lorentz force acting on the vortex and l is the vortex length. From this follows that the behavior of the probability function ν_a, and thus also $\rho_{\parallel,a}$, is anisotropic and depends only on the variables T, F, and α. The behavior of ν_i, on the other hand, is more complicated and depends additionally on the nonlinear $\nu_a(T,F)$ function.

We are now set to give explicit expressions for the temperature dependence of $\ln \rho_{\parallel}$. Taking into account that $\tan^2 \alpha$ competes with ν_a in $\rho_{\parallel a}$ [Eq. (38)] and with ν_a^2 in the $F_i(\alpha)$ dependence [Eq. (41)], one can distinguish three different limiting cases using the form for the probability functions ν_a and ν_i proposed in Eq. (40) and simplify Eq. (39) in these cases to

$$\ln \rho_{\parallel} \approx \begin{cases} -(\theta/k_B T)\{(U_{0i}+U_{0a})-[b_i \nu_a (F\cos\alpha)-b_a]F\cos\alpha\}+\ln(\rho_N \cos^2\alpha),\ \tan^2\alpha \ll \nu_a^2 \\ -(\theta/k_B T)\{(U_{0i}+U_{0a})-(b_i \sin\alpha + b_a \cos\alpha)F\},\ \nu_a^2 \ll \tan^2\alpha \ll \nu_a \\ -(\theta/k_B T)(U_{0i}-Fb_i \sin\alpha)+\cot^2\alpha \cdot \nu_a (F\cos\alpha)+\ln(\rho_N \sin^2\alpha),\ \nu_a \ll \tan^2\alpha < \infty. \end{cases} \quad (42)$$

The first limiting case is $\nu_a \ll \tan^2\alpha < \infty$. Because $\nu_a \leqslant 1$ always, this relation is realized for large enough angles α in the whole temperature range. This condition is also fulfilled for smaller angles at low temperatures and currents where the probability function $\nu_a \to 0$. It follows that

$$\ln \rho_{\parallel}(T) \approx (-\theta/k_B T)(U_{0i}-Fb_i \sin\alpha)+\ln(\rho_N \sin^2\alpha), \quad (43)$$

if one neglects the second term in the corresponding case in Eq. (42). Consequently, the Arrhenius plot will show a linear behavior for large enough angles over the whole temperature range. Indeed, the Arrhenius plot for $\alpha=90°$ and 60° can be fitted very well with a straight line over the whole temperature range for a magnetic field of $\mu_0 H=15$ mT (see Fig. 9) and is also linear in the low-temperature region (i.e., the right part of the Arrhenius plot) for magnetic fields of $\mu_0 H=7$ and 30 mT (see Figs. 8 and 10).

The next limiting case is $\nu_a^2 \ll \tan^2\alpha \ll \nu_a$. This condition is more complicated. It corresponds to moderate temperatures and low angles. $\nu_a \ll 1$, and thus $\nu_a \gg \nu_a^2$ at low enough temperatures; additionally, the angle α must be small enough and the probability function ν_a must be large enough to satisfy the condition $\nu_a^2 \ll \tan^2\alpha \ll \nu_a$. As can be seen from Eq. (42), the Arrhenius plot of $\ln \rho_{\parallel}$ is also linear in this case but the slope differs from the value of $(U_{0a}-Fb_a \cos\alpha)$, as was obtained in the previous case.

In the last case, the condition $\tan^2\alpha \ll \nu_a^2$ holds. This case can be realized at small angles and at high temperatures ($\nu_a \to 1$ for $T \to T_c$). From Eq. (42) follows that $\ln \rho_{\parallel}(T) \approx -(\theta/k_B T)\{(U_{0i}+U_{0a})-[b_i \nu_a (F\cos\alpha)-b_a]F\cos\alpha\}+\ln(\rho_N \cos^2\alpha)$. This dependence contains the term $(\theta/k_B T)\times[b_i \nu_a (F\cos\alpha)-b_a]F\cos\alpha$ which will cause a nonlinearity of the Arrhenius plot in the temperature and angle regions within its validity range. The nonlinearity is caused by the nonlinear dependence of the probability function ν_a on the temperature. This nonlinear dependence of $\ln \rho_{\parallel}$ is observed in Figs. 8–10, near T_c for small values of the angle α. For clarity, the Arrhenius plot of the longitudinal magnetoresistivity in a magnetic field of $\mu_0 H=15$ mT for the temperature range of 8.39 K $> T >$ 8.29 K is shown in the inset of Fig. 9.

We want to conclude this analysis by quantifying the remaining parameters of the assumed pinning scenario. We will again refer to the Arrhenius plot for a magnetic field of $\mu_0 H=15$ mT. Using Eq. (43) for two different transport current orientations, large enough α, and low temperatures, so that the condition $\tan^2\alpha \gg \nu_a$ is satisfied, one can estimate the value of the term Fb_i and the depth of the pinning potential well U_{0i}. It is easy to see that for two different angles α_1 and α_2,

$$Fb_i = [U_{\mathrm{eff}}(\alpha_1)-U_{\mathrm{eff}}(\alpha_2)]/(\sin\alpha_2-\sin\alpha_1),$$

$$U_{0i} = [U_{\mathrm{eff}}(\alpha_1)\sin\alpha_2 + U_{\mathrm{eff}}(\alpha_2)\sin\alpha_1]/(\sin\alpha_2-\sin\alpha_1), \quad (44)$$

with $U_{\mathrm{eff}}=U_{0i}-Fb \sin\alpha$ being the activation energy deduced from the Arrhenius plot. Taking the angles $\alpha_1=90°$ and $\alpha_2=60°$ and the corresponding U_{eff} from Table I, we obtain

$$Fb_i = 619 \text{ K},$$

$$U_{0i} = 1568 \text{ K}. \quad (45)$$

Note that for this estimate, the term depending on the ν_a function is neglected in Eq. (42).

If the transport current flows perpendicular to the magnetic field, the Lorentz force F acting on the vortex can be estimated using $F=l(J\cdot\Phi_0)$. Taking $l=25$ nm corresponding to the film thickness and $J=8\text{kA/cm}^2$, one obtains $F=4.14\times10^{-15}N$. Taking furthermore into account the estimate in Eq. (45), the following value for the characteristic width of the isotropic pinning potential is obtained: $b_i \approx 2$ μm. If we assume a characteristic width of the anisotropic pinning potential of about half the facet period length $b_a \approx 200$ nm, the value of Fb_a can be estimated as $Fb_a \approx 60$ K, which is much smaller than the measured activation energies U_{eff} (see Table I). For the estimation of the depth of the potential well U_{0a}, the Arrhenius plot for the $\alpha=0°$ transport current orientation is considered. The relation $\tan^2\alpha \ll \nu_a^2$ can be satisfied at temperatures near T_c and the corresponding expression for $\ln \rho_{\parallel}$ from Eq. (42) can be used. Because of the arguments stated above, the term $[b_i \nu_a (F\cos\alpha)-b_a]F\cos\alpha$ can be neglected and $\ln \rho_{\parallel} \approx -(\theta/k_B T)(U_{0a}+U_{0i})$, and thus $U_{\mathrm{eff}} \approx (U_{0a}+U_{0i})$ for this geometry. The thus obtained estimation gives the value of the depth of the potential well for the anisotropic pinning $U_{0a}=4031$ K. From the previously estimated value for $Fb_a \approx 60$ K, we see that the employed current density of $J=8$ kA/cm^2 places our experiments in the weak-current limit except for temperatures very close to T_c.

We are now in the position to calculate the complete temperature dependence of the longitudinal magnetoresistivity in Arrhenius representation using as probability functions ν_a and ν_i the function obtained for the triangle model potential and the corresponding parameters U_0 and b for the isotropic and anisotropic pinning potentials, as estimated. The ν_a and ν_i functions were additionally normalized so that $\nu_{a,i}(T_c)=1$ for the calculations. This turned out to be necessary because the studied system has a large activation energy and, in the proposed theoretical model, the critical temperature is defined via the pinning potential $k_B T_c = U_0$, which cannot be realized in the experiment. The best fit of the experimental

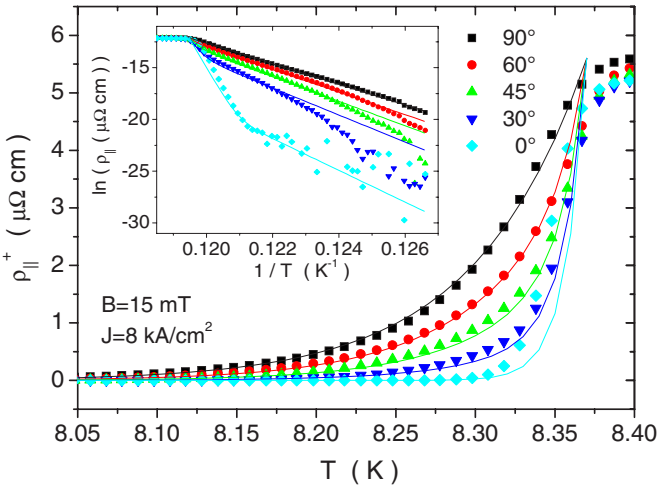

FIG. 11. (Color online) Calculated (line) and measured (data points) dependencies of the even longitudinal magnetoresistivity on the temperature and its Arrhenius plot (inset). The parameters for the calculated dependencies are as follows: $U_{0a}=4031$ K, $U_{0i}=1568$ K, $b_i/b_a=15$, and $\delta\alpha=-3°$.

data was obtained for $b_i/b_a=15$ and an assumed misalignment of α of about $-3°$, which is very well within the estimated alignment accuracy for the structure used. The result appears in Fig. 11. A comment is in order with regard to the characteristic width $b_a=b_i/15\approx 130$ nm. This coincides with the average width of the $(10\bar{1}\bar{2})$ facet for the observed average facet period length of 400 nm.

V. SUMMARY

In the present work, the phenomenon of vortex guiding in the mixed state of type-II superconductors was described based on a theoretical stochastic approach. A detailed comparison of the theoretical results with vortex guiding phenomena in epitaxial Nb thin films grown on faceted, *m*-cut α-Al_2O_3 surfaces was performed. For films of 25 nm thickness, guiding caused by the pinning action of the facet structure was clearly seen both in the longitudinal and transverse components of the magnetoresistivity tensor. A quantitative agreement between the theoretical description of guiding within a stochastic approach with the experimental data could be achieved. In this regard, the superconductor-on-facet structure topology may be considered to be a model system for studying guiding effects, in particular, in the nonlinear regime. The observed anomalous Hall effect remains as an open issue i.e., its sign change as a function of temperature. Although explicable within the theoretical approach, its origin cannot simply be traced back to a guiding phenomenon since an anomalous Hall effect can also occur in Nb layers on flat substrate surfaces. It also has to be mentioned that the true nature of the vortex state in the Nb films at $T\ll T_c$ may not be adequately described by the thermally activated flux-flow model. Yet, this does not invalidate the comparison of our experimental data at $(T_c-T)\ll T_c$ with the predictions of the stochastic approach. It rather may signify the need to repeat this analysis once the true vortex state in Nb films at low temperatures is elucidated. This has to remain for future resolution.

ACKNOWLEDGMENT

This work was partially supported by the Deutsche Forschungsgemeinschaft (DFG) through Grant No. 436 UKR 17/18/05.

*sorka@physik.uni-frankfurt.de

[1] A. K. Niessen and C. H. Weijsenfeld, J. Appl. Phys. **40**, 384 (1969).
[2] S. Fleshler, W. K. Kwok, U. Welp, V. M. Vinokur, M. K. Smith, J. Downey, and G. W. Crabtree, Phys. Rev. B **47**, 14448 (1993).
[3] W. K. Kwok, U. Welp, G. W. Crabtree, K. G. Vandervoort, R. Hulscher, and J. Z. Liu, Phys. Rev. Lett. **64**, 966 (1990).
[4] G. Blatter, M. V. Feigelman, V. B. Geshkenbein, A. I. Larkin, and V. M. Vinokur, Rev. Mod. Phys. **66**, 1125 (1994).
[5] A. A. Prodan, V. A. Shklovskij, V. V. Chabanenko, A. V. Bondarenko, M. A. Obolenskii, H. Szymczak, and S. Piechota, Physica C **302**, 271 (1998).
[6] V. V. Chabanenko, A. A. Prodan, V. A. Shklovskij, A. V. Bondarenko, M. A. Obolenskii, H. Szymczak, and S. Piechota, Physica C **314**, 133 (1999).
[7] H. Pastoriza, S. Candia, and G. Nieva, Phys. Rev. Lett. **83**, 1026 (1999).
[8] G. D'Anna, V. Berseth, L. Forro, A. Erb, and E. Walker, Phys. Rev. B **61**, 4215 (2000).
[9] V. Berseth, Ph.D. thesis, EPFL, 1999.
[10] Y. Mawatari, Phys. Rev. B **56**, 3433 (1997).
[11] Y. Mawatari, Phys. Rev. B **59**, 12033 (1999).
[12] V. A. Shklovskij, A. A. Soroka, and A. K. Soroka, J. Exp. Theor. Phys. **89**, 1138 (1999).
[13] V. A. Shklovskij, Phys. Rev. B **65**, 092508 (2002).
[14] V. A. Shklovskij and A. A. Soroka, J. Low Temp. Phys. **130**, 407 (2003).
[15] V. A. Shklovskij, Physica B **248**, 825 (2000).
[16] V. A. Shklovskij, Physica C **388-389**, 655 (2003).
[17] V. A. Shklovskij, J. Low Temp. Phys. **139**, 289 (2005).
[18] O. K. Soroka, Ph.D. thesis, Johannes Gutenberg University, Mainz, 2005.
[19] G. W. Crabtree, D. O. Gunter, H. G. Kaper, A. E. Koshelev, G. K. Leaf, and V. M. Vinokur, Phys. Rev. B **61**, 1446 (2000).
[20] B. Chen and J. Dong, Phys. Rev. B **44**, 10206 (1991).
[21] O. V. Usatenko and V. A. Shklovskij, J. Phys. A **27**, 5043 (1994).
[22] V. M. Vinokur, V. B. Geshkenbein, M. V. Feigel'man, and G. Blatter, Phys. Rev. Lett. **71**, 1242 (1993).
[23] V. A. Shklovskij and O. V. Dobrovolskiy, Phys. Rev. B **74**, 104511 (2006).
[24] V. A. Shklovskij, J. Low Temp. Phys. **131**, 899 (2003).
[25] See, e.g., A. Wildes, J. Mayer, and K. Theis-Bröhl, Thin Solid Films **201**, 7 (2001).
[26] L. Wiehl, J. Oster, and M. Huth, J. Appl. Crystallogr. **38**, 260

(2005).
[27] W. W. Mullins, Philos. Mag. **6**, 1313 (1961).
[28] E. D. Williams and N. C. Bartelt, Science **251**, 393 (1991).
[29] R. J. Phaneuf and E. D. Williams, Phys. Rev. Lett. **58**, 2563 (1987).
[30] O. Kurnosikov, L. Pham Van, and J. Cousty, Surf. Interface Anal. **29**, 608 (2000).
[31] C. Herring, Phys. Rev. **82**, 87 (1951).
[32] V. A. Shchukin and D. Bimberg, Rev. Mod. Phys. **71**, 1125 (1999).
[33] S. Ramamurthy, B. C. Herbert, and C. B. Carter, Philos. Mag. Lett. **72**, 269 (1995).
[34] M. Huth, K. A. Ritley, J. Oster, H. Dosch, and H. Adrian, Adv. Funct. Mater. **12**, 333 (2002).
[35] J. Oster, L. Wiehl, H. Adrian, and M. Huth, J. Magn. Magn. Mater. **292**, 164 (2005).
[36] J. Oster, M. Kallmayer, L. Wiehl, H.-J. Elmers, H. Adrian, F. Porrati, and M. Huth, J. Appl. Phys. **97**, 014303 (2005).
[37] J. R. Heffelfinger and C. B. Carter, Surf. Sci. **343**, L1161 (1995).
[38] J. R. Heffelfinger and C. B. Carter, Surf. Sci. **389**, 188 (1997).
[39] J. Oster, Ph.D. thesis, Johannes Gutenberg University, Mainz, 2004.
[40] T. T. M. Palstra, B. Batlogg, L. F. Schneemeyer, and J. V. Waszczak, Phys. Rev. Lett. **61**, 1662 (1988).
[41] C. Ren, F. Y. Lin, Z. M. Li, S. A. Aruna, L. Qui, X. X. Yao, S. L. Yan, and M. S. Si, Supercond. Sci. Technol. **12**, 400 (1999).
[42] Isotropic pinning which is usually present in real system and leads to the existence of a nonzero critical current in this geometry will be dealt with in the next section.
[43] The superscript "+" is left out here and in all the following formulas for the even longitudinal component $\rho_{\|}^{+}$ to simplify the notation.